IEEE Access
Multidisciplinary | Rapid Review | Open Access Journal

Received October 30, 2019, accepted November 25, 2019, date of publication December 5, 2019,
date of current version December 23, 2019.

Digital Object Identifier 10.1109/ACCESS.2019.2957877

Noise Suppression Method of Microseismic Signal Based on Complementary Ensemble Empirical Mode Decomposition and Wavelet Packet Threshold

LING-QUN ZUO[1], HONG-MEI SUN[1,2], QI-CHAO MAO[1], XIAO-YING LIU[1], AND RUI-SHENG JIA[1,2]

[1]College of Computer Science and Engineering, Shandong University of Science and Technology, Qingdao 266590, China
[2]Shandong Province Key Laboratory of Wisdom Mine Information Technology, Shandong University of Science and Technology, Qingdao 266590, China

Corresponding authors: Hong-Mei Sun (shm0221@163.com) and Rui-Sheng Jia (jrs716@163.com)

This work was supported in part by the Key Research and Development Program of Shandong Province, China, under Grant 2017GSF20115, and in part by the Natural Science Foundation of Shandong Province, China, under Grant ZR2018MEE008.

ABSTRACT Aiming at the situation that complementary ensemble empirical mode decomposition (CEEMD) noise suppression method may produce redundant noise and wavelet transform easily loses high-frequency detail information, considering wavelet packet transform can be used to perform better time-frequency localization analysis on signals containing a large amount of medium and high frequency information, according to the noise and useful signal components of both the characteristic of self-correlation function is different, the CEEMD and wavelet packet threshold jointed method is proposed. The method uses the energy concentration ratio to find noise and useful signal component demarcation point to denoise the microseismic signals. Firstly, we utilize adaptively decompose the signal from high frequency to low frequency by the CEEMD; Secondly, using the self-correlation method to select the intrinsic mode function (IMF) that needs noise suppression, the wavelet suppression method is used to suppress the noise of several high-frequency components whose self-correlation coefficient is below the critical value K; Finally, the IMF component after the wavelet packet threshold noise suppression is reconstructed with the noise-free IMF component. In order to verify the effectiveness of the proposed method on the noise suppression of microseismic signal, we added a Gaussian white noise to the Ricker wavelet signal similar to the microseismic signal. The experimental results show that the signal-to-noise ratio (SNR) of the signal is raised more than 10dB. The energy percentage is higher than 92%. In practical engineering, our proposal achieves an effective noise suppression effect on the microseismic signal.

INDEX TERMS Complementary ensemble empirical mode decomposition, wavelet packet threshold, self-correlation, noise suppression.

I. INTRODUCTION

As the mining intensity of coal mines has increased year by year, the impact of coal mine power disasters has become more and more fierce, which has aggravated the impact of ground pressure and increased mine pressure. The mine operators have faced great challenges in coal mine safety issues. In the last century, micro-seismic monitoring technology of digital mines began to emerge. Many countries have established mine microseismic monitoring networks, which have been widely used in earthquake pressure prediction [1]–[4]. Because the coal rock damage is mostly micron-level vibration intensity, the signal is very weak, and the external noise causes the received signal to always be mixed with noise, which makes the signal's effectiveness greatly reduced [5]–[9]. In order to improve the effectiveness of coal and rock microseismic signals, it is necessary to make full use of noise suppression means to suppress the signal [10]–[14]. The noise suppression of the noisy microseismic signal can better provide real and effective signals to reduce the noise

The associate editor coordinating the review of this manuscript and approving it for publication was Jenny Mahoney.

signal interference for the subsequent work such as the initial phase picking, the source location, and the focal mechanism interpretation.

Microseismic signals are characterized by randomness and non-stationarity. Many signal noise reduction methods have been proposed, among which the empirical mode decomposition method and wavelet transform method are the two methods that have great influence [15]–[21]. In the coal rock microseismic signal, the noise is concentrated in the high frequency part, and the useful signal is concentrated in the low frequency part. EMD(Empirical mode decomposition) can decompose the signal into a series of sub-signals of IMF. Each IMF is a different function component, which can describe the input signal at different scales. After Hilbert transform, the instantaneous properties with obvious physical meaning can be obtained [21]–[23]. Meanwhile, EMD has the characteristics of orthogonality, self-adaptation completeness, etc., and is suitable for nonlinear analysis. However, when the IMF component of a certain frequency band in the signal is discontinuous or there is intermittent signal noise interference, modal aliasing occurs, which reduces the accuracy of the decomposition. In order to solve the modal aliasing phenomenon, Peng Ping et al. proposed the EEMD(Ensemble empirical mode decomposition), by adding white noise to the signal, changing the signal extreme point distribution, and obtaining the upper and lower envelopes in accordance with the signal characteristics, eliminating the modal aliasing effect, but EEMD is not good for signal reconstruction [24]. The CEEMD method can effectively solve the problem of large reconstruction error caused by noise pollution in the EEMD method by adding positive and negative paired auxiliary noise. The essential decomposition process of the CEEMD method has not changed. It is still independent of EMD decomposition after adding positive and negative pairs of auxiliary noise. Finally, the corresponding order IMF component of each implementation is used as the final result, but its decomposition. Part of the random noise information still exists in the obtained single IMF component, and the improper setting of the auxiliary noise parameter will cause the number of IMF components to be inconsistent.

The wavelet transform method is suitable for non-stationary and nonlinear signals and also has advantages in local information processing. Some scholars have proposed combining the CEEMD method with the wavelet transform method to perform noise suppression on microseismic signals. Compared with the single CEEMD method and the separate wavelet transform method, this combination method has a better effect on the suppression of micro seismic signal noise [25], [26]. However, using the wavelet transform method to perform threshold denoising on the high-frequency IMF component decomposed by CEEMD still loses some high-frequency detail information, and the useful signal is still incomplete. And the wavelet transform method adaptability is poor. When wavelet decomposition is performed, only low frequency is decomposed, resulting in high-frequency detail information loss. The wavelet packet transform can provide a more detailed decomposition of the signal, and this decomposition has neither redundancy nor omission, so it can also perform better time-frequency localization analysis on signals containing a large amount of medium and high frequency information.

Therefore, we proposed the CEEMD global threshold and wavelet packet transform combined noise suppression method based on self-correlation function to suppress the noise of coal rock microseismic signals. The idea is as follows: Firstly, the CEEMD method is used to decompose the micro-seismic signals of the noisy coal rock into several IMF components. Secondly, the IMF component with more noise is determined by the characteristics of self-correlation function, and then we use the wavelet packet threshold method to suppress the noise of the IMF component with more noise. Finally, the IMF component after wavelet packet threshold denoising is reconstructed from the remaining IMF component after CEEMD decomposition without noise suppression, to achieve the purpose of noise suppression.

II. RELATED WORK

A. CEEMD PRICIPLE

CEEMD is based on the improved EMD method, which overcomes the modal aliasing problem of EMD and retains the processing advantages of EMD for nonlinear signals. The CEEMD method adds auxiliary noise in the form of positive and negative pairs, which eliminates the residual auxiliary noise in the reconstructed signal, and the number of added noise sets can be low and the calculation efficiency is high. CEEMD includes the following steps:

Step 1 : Add n sets of auxiliary white noise in positive and negative pairs in the original signal to generate two sets of IMFs.

$$\begin{pmatrix} m_1 \\ m_2 \end{pmatrix} = \begin{pmatrix} 1 & 1 \\ 1 & -1 \end{pmatrix} \begin{pmatrix} x(t) \\ n(t) \end{pmatrix} \tag{1}$$

where $x(t)$ is the original signal; $n(t)$ is the auxiliary noise, the amplitude of which can be selected from 0.2 to 0.5 times the standard deviation of the original signal or can be appropriately adjusted and increased with the intensity of the noise; The m_1 and m_2 are respectively added to the positive and negative paired noise signal, so that the number of sets of signals is $2n$;

Step 2: EMD decomposition is performed on each signal in the set, and each signal obtains a series of IMF components, where in *j-th* IMF component of the *i-th* signal is $imf_{ij}(t)$;

Step 3: Then average the multi-component quantity combination

$$imf_j(t) = \frac{1}{2n} \sum_{i=1}^{2n} imf_{ij}(t) \tag{2}$$

where $imf_j(t)$ is the *j-th* IMF component of the signal after CEEMD decomposition. The method ensures the completeness of the signal decomposition, can better solve the modal aliasing effect, and the calculation efficiency is greatly improved.

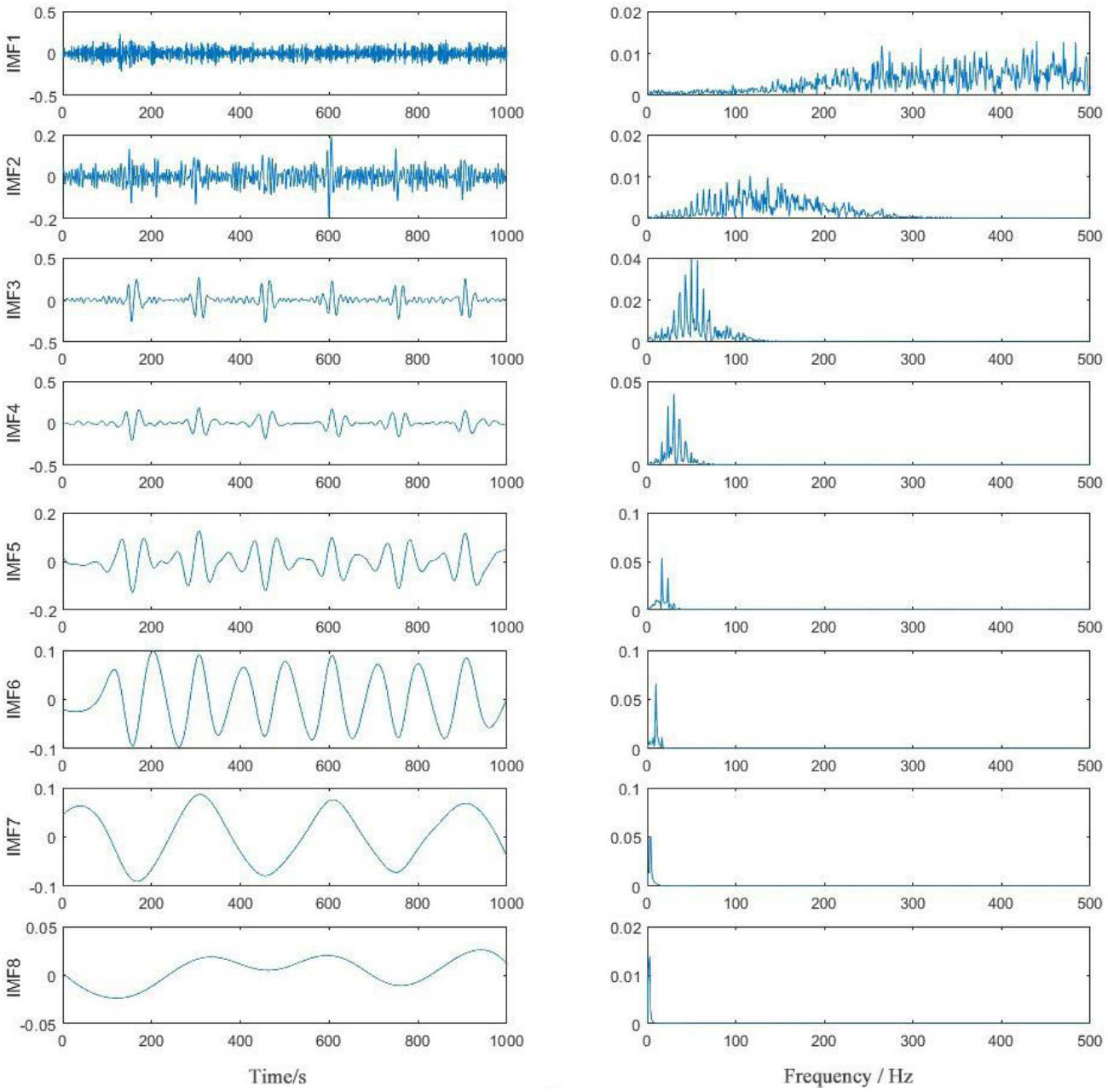

FIGURE 1. CEEMD decomposition results and their corresponding spectrum.

In this paper, CEEMD is used to decompose the original noisy signal into multiple IMF components, and then use the wavelet packet threshold method to perform noise suppression. We can visually see from Fig. 1 that each IMF component and spectrogram of the noisy signal after CEEMD decomposition.

B. THE PRINCIPLE OF WAVELET PACKET NOISE SUPRESSION

The basic principle of wavelet packet threshold denoising is to first decompose the input signal into wavelet packet, obtain the wavelet packet coefficient. And then select an appropriate threshold, and process the coefficients generated after the wavelet packet decomposition according to the threshold function. If the wavelet packet coefficient is smaller than Threshold, the wavelet packet coefficient is considered to be caused by noise, and the partial coefficient is removed. If the wavelet packet coefficient is greater than the threshold, then the coefficient is considered to be caused by the signal, and the wavelet packet coefficient is retained. Finally, the wavelet packet coefficients obtained after thresholding are reconstructed to obtain the denoised signal.

The formula for a continuous wavelet transform for any function is:

$$WT_x(a,b) = \frac{1}{\sqrt{|a|}} \int_{-\infty}^{+\infty} x(t)\psi^*\left(\frac{t-b}{a}\right) dt \qquad (3)$$

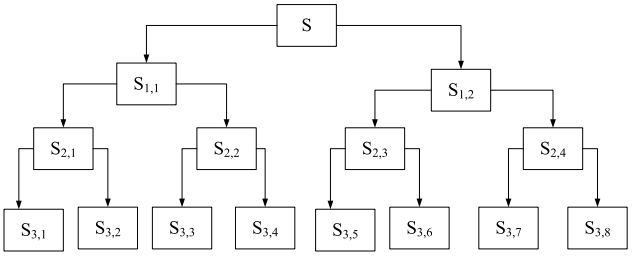

FIGURE 2. Schematic diagram of wavelet packet decomposition.

where $\psi^*(t)$ is the conjugate of the mother wavelet function; a is the scale parameter; b is the translation parameter; $WT_x(a, b)$ is the continuous wavelet transform.

In the continuous wavelet, the scale parameter a and the translation parameter b are discretized separately, and $a = a_0^j$, $b = ma_0^j b_0, j \in Z, m \in Z, a_0 \neq 1$ are taken.

Then the wavelet basis function is:

$$\psi_{j,k}(t) = a_0^{-j/2}\psi\left(a_0^{-j}t - mb_0\right) \tag{4}$$

Discrete wavelet transform:

$$WT_x(j, m) = \int_{-\infty}^{+\infty} x(t)\psi_{j,m}^*(t)\,dt \tag{5}$$

Wavelet decomposition is an effective time-frequency analysis method, its disadvantage is that it only partially decomposes the low-frequency information, but the high-frequency components are not processed, so the resolution is poor. The wavelet packet further decomposes the undecomposed high frequency portion, and the time-frequency resolution is improved. Therefore, wavelet packet decomposition is a more effective method [27]–[31].

The function calculation method of wavelet packet decomposition is:

$$\begin{cases} d_{i,j,2n} = \sum_n h(k-2i)\, d_{k,j+1,n} \\ d_{i,j,2n+1} = \sum_n g(k-2i)\, d_{k,j+1,n} \end{cases} \tag{6}$$

The calculation method of the reconstruction function of the wavelet packet is:

$$d_{i,j+1,2n} = \sum_n h(i-2k)\, d_{k,j,n} + \sum_n g(k-2i)\, d_{k,j+1,n} \tag{7}$$

where $d_{i,j,2n}$ is the *i-th* wavelet packet coefficient of the nth node of the *j-th* layer; $h(k)$ and $g(k)$ are the expansion coefficients.

Figure 2 is a schematic diagram of three-layer wavelet packet decomposition. Through experimental analysis, we decompose the signals with 2, 3, 4, and 5 layers respectively, and find that the signal-to-noise ratio (SNR), energy percentage (ESN), and root mean square error are the highest. RMSE) is the smallest, so the 3-layer decomposition is chosen to achieve the desired effect. S is the original signal, $S_{1,1}$ is the high frequency component, $S_{1,2}$ is the low frequency component, $S_{1,1}$ is further divided into $S_{2,1}$, $S_{2,2}$; $S_{1,2}$ is further divided into $S_{2,3}$, $S_{2,4}$; according to this rule, it is sequentially decomposed step by step.

After the signal S is decomposed by the n-layer wavelet packet, it can be expressed as:

$$S = S_{N.1} + S_{N.2} + \ldots + S_{N.2^N-1} + S_{N.2^N} \tag{8}$$

In formula (8), $S_{N.1}, S_{N.2}, \ldots, S_{N.2^N-1}, S_{N.2^N}$ represents 2^N sub-bands decomposed by the n-layer wavelet packet. The 2^N sub-bands effectively retain the useful part of the original signal. The noise is concentrated in the high-frequency part, but the low-frequency part still retains part of the noise. Therefore, the wavelet packet threshold noise reduction must be performed on the 2^N sub-bands.

The wavelet packet threshold method is extremely important in terms of threshold selection. Soft threshold method and hard threshold method have good noise suppression effect in practical applications, but the traditional soft and hard threshold noise suppression adopts fixed threshold method, which has many shortcomings [32]. The hard threshold is widely used because it can effectively maintain the signal amplitude, but the hard threshold reconstruction signal is discontinuous at the threshold point and will oscillate, and there is a Pseudo-Gibbo phenomenon. The soft threshold method overcomes the shortcomings of signal discontinuity, but does not have the advantage of maintaining a hard threshold. There is a constant deviation between the wavelet estimation coefficient and the wavelet coefficient [33]. Both the soft threshold method and the hard threshold method have discontinuities and signal distortion problem.

We assume that $\omega_{i,t}$ is the original wavelet packet coefficient, $\hat{\omega}_{j,k}$ is the wavelet packet coefficient after thresholding, i and t are wavelet packet nodes, λ is the threshold, and $sgn(\omega_{it})$ is the sign function. The soft and hard threshold function expressions are as follows:

The hard threshold function is:

$$\begin{cases} \hat{\omega}_{i,t} = \omega_{it}, & |\omega_{it}| \geq \lambda \\ \hat{\omega}_{i,t} = 0, & |\omega_{i,t}| < \lambda \end{cases} \tag{9}$$

The soft threshold function is:

$$\begin{cases} \hat{\omega}_{i,t} = sgn(\omega_{it})\left(|\omega_{it}| - \lambda\right), & |\omega_{it}| \geq \lambda \\ \hat{\omega}_{i,t} = 0, & |\omega_{i,t}| < \lambda \end{cases} \tag{10}$$

In order to eliminate the problem of soft threshold noise suppression method and hard threshold noise suppression method, scholars have proposed an improved threshold function [34]:

$$\begin{cases} \hat{\omega}_{it} = sgn\left(\omega_{i,t}\right)\left(|\omega_{i,t}| - \alpha\lambda\right), & |\omega_{i,t}| \geq \lambda \\ \hat{\omega}_{it} = 0, & |\omega_{i,t}| < \lambda \end{cases} \tag{11}$$

When $\alpha \to 0$, the threshold function is a hard threshold; when $\alpha \to 1$, the threshold function is a soft threshold function. This function is actually a soft-hard threshold compromise function, and different noise suppression effects can be obtained by adjusting the value.

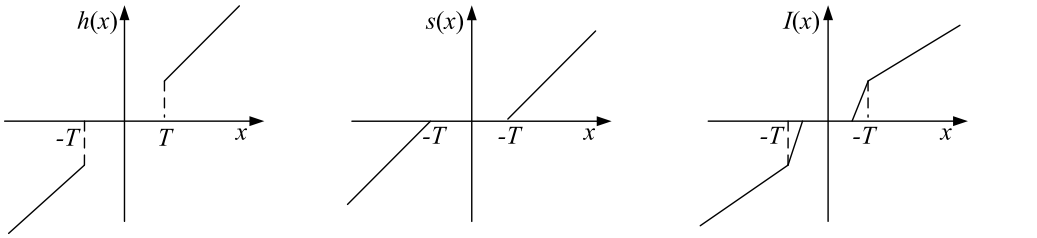

（1）Hard threshold method　（2）Soft threshold method　（3）Improved threshold method

FIGURE 3. Comparison of three wavelet threshold functions.

The three threshold functions of the hard threshold method, the soft threshold method and the improved threshold method are shown in Figure 3, in which the abscissa is the original wavelet coefficient and the ordinate is the coefficient obtained by the threshold function processing.

C. SELF-CORRELATION ANALYSIS

According to the decomposition step of CEEMD in section 1.1, the signal is decomposed into IMF components with frequencies from high to low. In actual engineering, the noise tends to be characterized by high frequency. If the boundary point K of the high frequency and low frequency IMF components can be determined and the useful signal contained in the high frequency IMF can be picked up, the useful signals can be reconstructed by superimposing the low frequency IMF to achieve the noise suppression purposes. In this paper, the different characteristics of the noise signal and the useful signal self-correlation function are used. The boundary point K is determined by combining the energy ratio, and the noisy signal IMF component to be processed is obtained [35].

1) SELF-CORRELATION FUNCTION AND ENERGY CONCENTRATION RATIO

The self-correlation function of the random signal reflects the degree of similarity between the signal and its own at different points in time. It is a measure of the time domain and is defined as:

$$R_x(t_1, t_2) = E[x(t_1)x(t_2)] \tag{12}$$

where a is a random signal and the normalized self-correlation function appears as:

$$\rho_x(t_1, t_2) = \frac{R_x(t_1, t_2)}{R_x(0)} \tag{13}$$

where $R_x(0)$ represents the value of the correlation function of the signal at the same time as itself. Obviously, any random signal has a maximum value.

It is considered that the white noise is different from the normalized self-correlation function of the general signal. The normalized self-correlation function value of random noise is the largest at zero, and the other points are immediately attenuated to zero. However, the general signal normalized self-correlation function value is the maximum at zero but does not immediately decay to zero, which is a process of slow decline. Since the randomness of the values of random noise at each time point is weakly correlated, the value of each time point of the general signal has a certain correlation, which is characterized by strong correlation.$h(x)T$

How to accurately determine the self-correlation of random signals from the whole, and give the definition of energy concentration ratio: the ratio of the energy of a random signal over a certain period of time to the energy of the whole signal, which is expressed as:

$$\eta_x(t_1, t_2) = \frac{E_x(t_1, t_2)}{E_x(t)} = \frac{\int_{t_1}^{t_2} x^2(t)\,dt}{\int_{t}^{\infty} x^2(t)\,dt} \tag{14}$$

where $x(t)$ is a random signal, if it is a discrete sequence, then equation (15) is expressed as:

$$\eta_x(n_1, n_2) = \frac{E_x(n_1, n_2)}{E_x(n)} = \frac{\sum_{n_1}^{n_2} x^2(n)}{\sum_{n} x^2(n)} \tag{15}$$

After the signal is decomposed by CEEMD, a set of IMF components is obtained. The normalized self-correlation function corresponding to the IMF component can be regarded as a set of random sequences. Calculating the energy concentration ratio of the interval near the zero point, the sequence can be judged to be at zero. The degree of energy concentration in the nearby interval, and then the magnitude of the self-correlation of the IMF components.

2) DETERMINATION OF THE K VALUE OF THE BOUNDARY POINT

Calculate the coefficient on the basis of equation (16):

$$\rho_j = \frac{\left|\eta_j(\mathrm{V}n) - \frac{1}{j-1}\sum_{i=1}^{j-1}\eta_i(\mathrm{V}n)\right|}{\eta_j(\mathrm{V}n)} \tag{16}$$

where $\eta_j(\mathrm{V}n)$ is the energy concentration ratio of the *j-th* IMF normalized self-correlation function on the interval $[\mathrm{V}-n, \mathrm{V}n]$. Obviously, if the first *j-1* IMFs are noise functions, then the value of ρ_{j-1} is close to 1, and the value of p is significantly larger than 1. Because it indicates that the self-correlation of the *j-th* IMF is less than half of the average value of the first *j-1* IMFs when $\rho_j \geq 1$. Accordingly, the first *j-1* IMFs are noise functions, and the cut-off point K is the j.

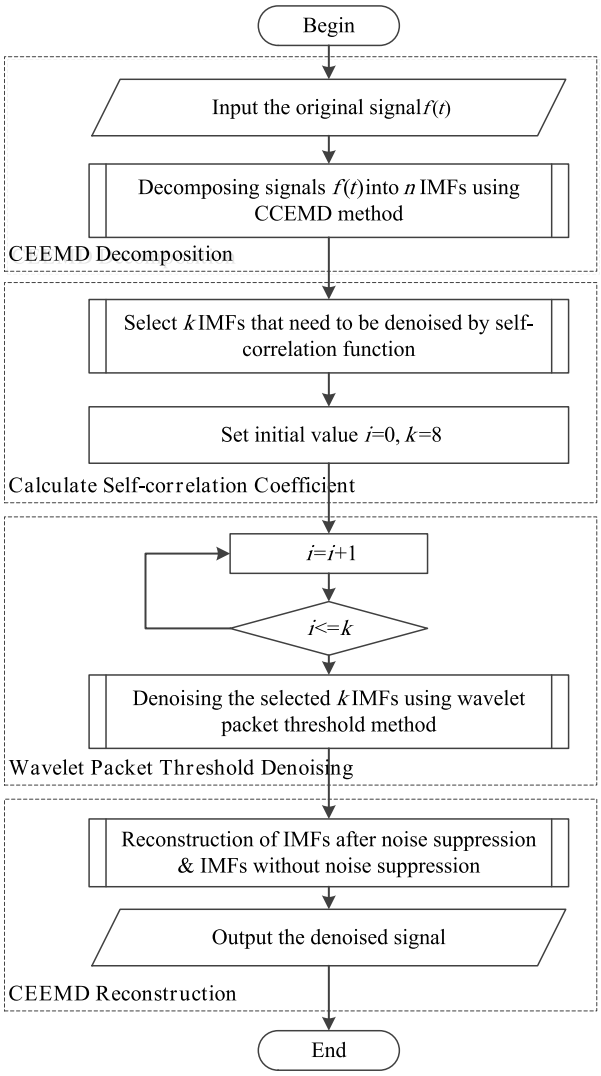

FIGURE 4. Flow chart of noise suppression based on CEEMD and wavelet packet threshold.

D. NOISE SUPPRESSION STEP

In this paper, CEEMD is combined with the wavelet packet threshold noise suppression method. The implementation steps of the noise suppression method are described as follows:

Step1: The original signal $f(t)$ is decomposed into n IMFs by CEEMD, which called as Ω, $\Omega = \{IMF_1, IMF_2, \ldots, IMF_n\}$.

Step2: Calculating the K value by self-correlation analysis to determine the IMFs that need to perform noise suppression, which called as δ, $\delta = \{IMF_1, IMF_2, \ldots, IMF_k\}$.

Step3: The wavelet packet improved threshold method is used to suppress the noise of the selected δ.

Step4: Reconstructing the noise-suppressed IMFs after the wavelet threshold noise suppression and the CEEMD-decomposed IMFs without noise suppression to obtain the noise-suppressed signal $I(t)$.

The flow chart is shown in Figure 4.

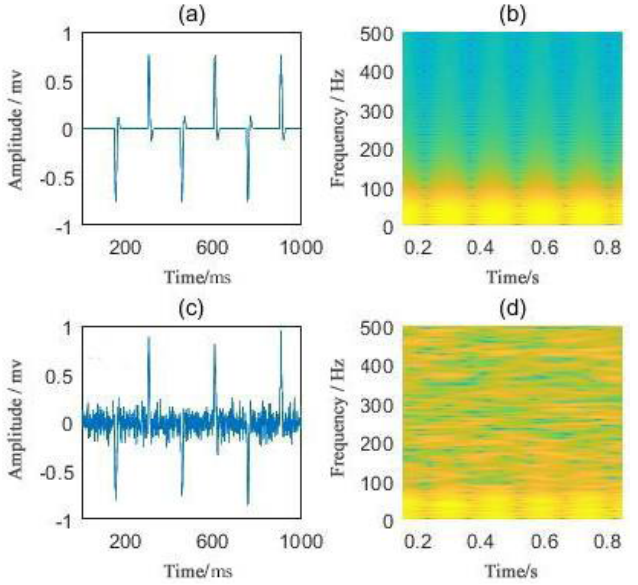

FIGURE 5. Ricker wavelet signal. (a) The waveform of signal $f(t)$; (b) The time spectrum of signal $f(t)$; (c) The waveform of signal $f'(t)$; (d) The time spectrum of signal $f'(t)$.

III. SIMULATION EXPERIMENT AND ANALYSIS

Since the Ricker wavelet has similar characteristics to the seismic signal, we use Ricker wavelet to verify the performance of the selected method. The mathematical expression of the synthetic Ricker wavelet can be expressed as:

$$s(t) = \exp\left(-\left(\frac{2\pi f_p}{r}t\right)^2\right)\cos 2\pi f_p t \tag{17}$$

where t represents time; f_p represents peak frequency; r represents wavelet width. In the simulation analysis, $f_p = 30$Hz, $r = 3$ is taken, the sampling frequency is 1000Hz, and the number of sampling points is 1000. Add Gaussian white noise to the simulated signal $f(t)$ to make its signal-to-noise ratio 5dB, which is recorded as $f'(t)$. The waveform of the simulated signal $f(t)$ and the noisy signal $f'(t)$ and its time spectrum are shown in Figure 5.

We use the CEEMD method, the wavelet packet threshold noise suppression method, and the method of this paper to suppress the noise of the noisy Ricker wavelet signal $f'(t)$, as shown in Figure 6.

Figure 6 shows that the noise suppression method of this paper is more stable than the CEEMD noise suppression method or the wavelet packet transform method. The noise-suppressed signal waveform is smoother than before without suppression. The noise-suppressed signal is basically consistent with the original signal in terms of overall characteristics and peak value, and the noise suppression effect is more obvious.

In order to further prove the noise suppression effect of we proposed in this paper, the signal-to-noise ratio (SNR), the root mean square error (RMSE) and energy percentage

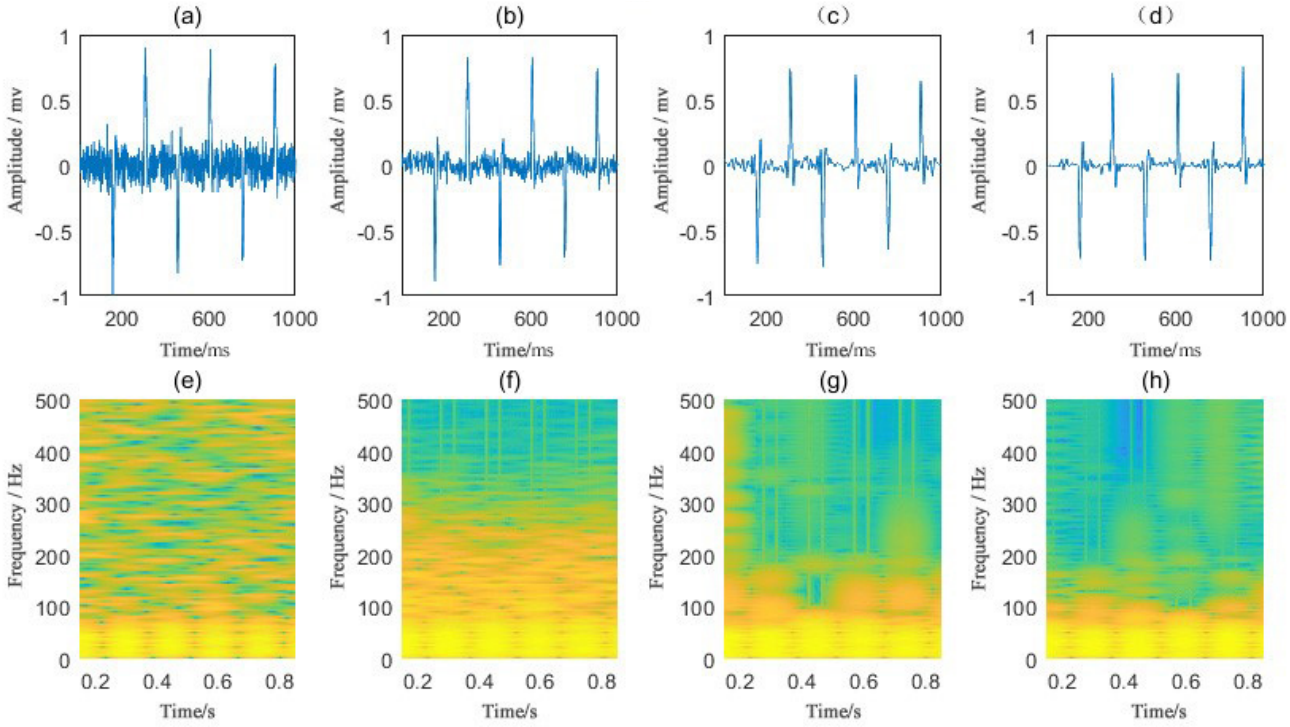

FIGURE 6. Comparison of three noise suppression for noisy Ricker wavelet. (a) The waveform of noisy signal; (b) Signal waveform after noise suppression using CEEMD method; (c) Signal waveform after the noise suppression using wavelet packet method; (d) Signal waveform after noise reduction using proposed method; (e) Time-frequency spectrum of noisy signal (a); (f) Time-frequency spectrum of signal (b); (g) Time-frequency spectrum of signal (c); (h) Time-frequency spectrum of signal (d).

TABLE 1. Comparison of noise Suppression results of three different methods.

Denoising method	SNR /dB		RMSE		E_{sn} /%
	Before denoising	After denoising	Before denoising	After denoising	
CEEMD	5	12.31	0.15	0.04	90.14
Wavelet packet	5	16.82	0.09	0.03	92.32
Proposed method	5	19.15	0.06	0.03	93.68

(E_{sn}) are used as indicators of noise suppression.

$$SNR = 10\log_{10}\left[\sum_{i=1}^{N}\frac{y_i^2}{(x_i - y_i)^2}\right] \tag{18}$$

The root mean square error formula is:

$$RMSE = \frac{1}{N}\sqrt{\sum_{N=1}^{N}|y_i - x_i|^2} \tag{19}$$

The formula for the energy percentage of the signal after noise suppression and the original signal is:

$$E_{sn} = \left(\sum_{i=1}^{N}|x_i|\right)\Big/\left(\sum_{i=1}^{N}|y_i|\right) \tag{20}$$

In equations (18), (19), and (20), y_i is the original signal, x_i is the signal after noise suppression, and N is the number of samples. The SNR, RMSE, and E_{sn} before and after the signal f noise suppression are calculated using equations (18), (19), and (20), respectively.

As shown in Table 1, the CEEMD, wavelet packet threshold method and the method of this paper respectively suppress the noise of the signal with 5 dB Gaussian white noise. Through the noise suppression signal of this method, the SNR and E_{sn} after noise suppression are obviously improved. The RMSE is significantly reduced.

TABLE 2. Noise suppression Results of four noisy signals.

Signal number	SNR(dB)		RMSE		Esn(%)
	Before denoising	After denoising	Before denoising	After denoising	
S1	0	12.49	0.15	0.03	90.23
S2	5	16.91	0.09	0.04	92.11
S3	10	22.67	0.05	0.03	93.19
S4	15	29.34	0.03	0.02	96.89

In order to quantitatively analyze the effect of the method, Gaussian white noise of F: 0, 5, 10, 15 (SNR/dB) is added respectively to verify the indicators, and then the effectiveness of the noise suppression method is demonstrated. We use F1, F2, F3 and F4 respectively to represent the noise adding 0, 5, 10, 15dB. Table 2 is quantitative analysis experiment.

It can be seen from Table 2 that after applying the method of we proposed, the SNR of the four groups of signals is

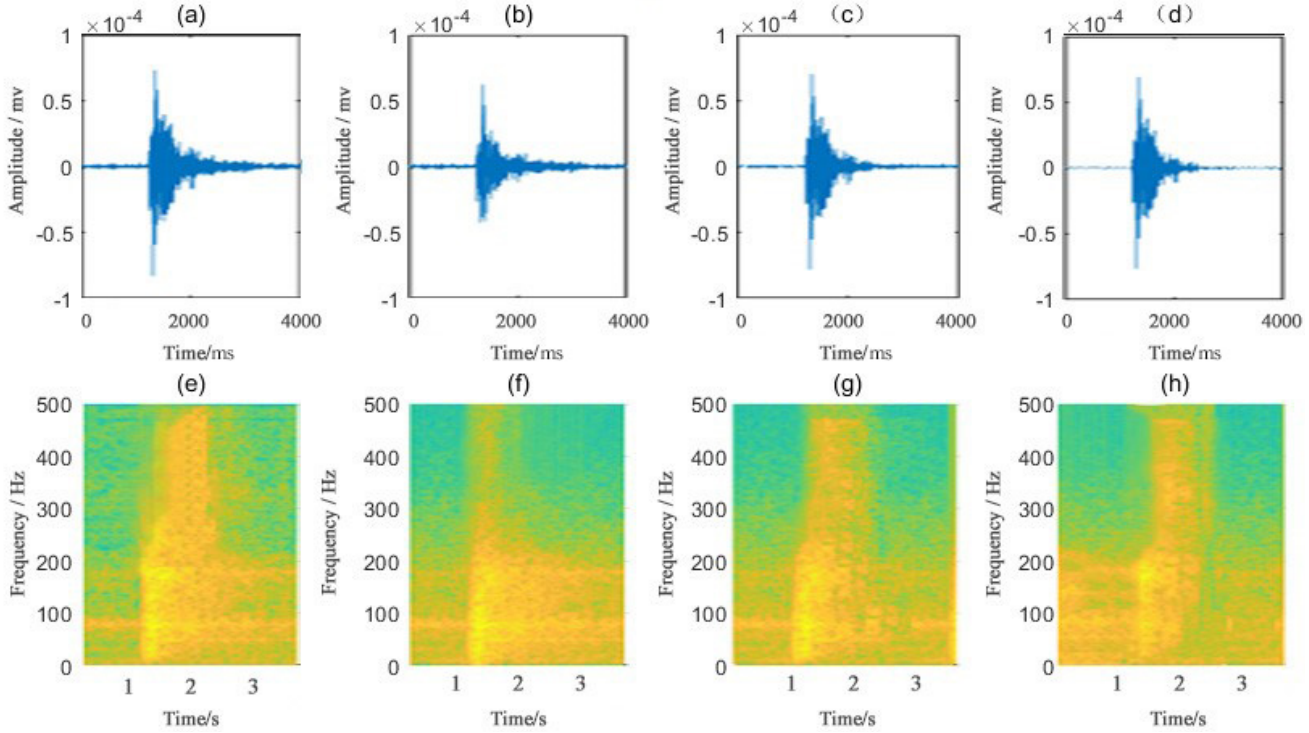

FIGURE 7. Comparison of three noise suppression for microseismic signals. (a) The original microseismic waveform of signal $g'(t)$; (b) The waveform of signal $g'(t)$ after noise suppression using CEEMD method; (c) Waveform of the signal $g'(t)$ after noise suppression using wavelet packet method; (d) The waveform of the signal $g'(t)$ after noise suppression using proposed method; (e) Time-frequency spectrum of signal $g'(t)$; (f) Time-frequency spectrum of signal (b); (g) Time-frequency spectrum of signal (c); (h) Time-frequency spectrum of signal (d).

increased to more than 10 dB, the RMSE is significantly smaller, and the energy percentage is maintained above 90%. Even in the case of a strong noise with SNR = 0 dB, the signal-to-noise ratio is increased to 11.344 dB, the root mean square error is reduced to 0.03, and the energy percentage is still maintained at 90.23%. It can be seen that the noise-reduced signals have higher signal-to-noise ratio, lower root mean square error and higher energy percentage, which proves the rationality and effectiveness of the noise suppression method.

IV. APPLICATION EXAMPLES

The experimental data comes from the microseismic monitoring data of a coal mine in central China. The sampling frequency of the signal is 1 kHz. Four noisy signals (Marked as S1, S2, S3, S4) are selected for comparative experimental analysis. Each group of signals is intercepted by the equal length of 4000 sampling points collected by the shock absorber. Take S1 as an example for analysis, and S1 is recorded as $g'(t)$. The CEEMD and wavelet packet thresholds are implemented by MATLAB programming. The proposed method performs noise suppression experiments on q respectively. The waveforms and time-frequency diagrams before and after noise reduction are shown in Figure 7.

It can be seen from Figure 7 that the time-spectrum (e) of the micro seismic signal $g'(t)$ contains a large amount of random noise. Although the dominant spectral distribution of the useful signal can be seen from the time spectrum, the dominant spectral distribution is not obvious due to noise interference. Submerged in the noise, this will cause interference to the subsequent calculation of the energy of the microseismic signal and the interpretation of the focal mechanism. Therefore, noise suppression processing is required. The microseismic signal waveform (d) is clearer than that before noise suppression and is better than the other two methods. The dominant spectrum distribution in the time spectrum is also more obvious. Do the same for S2, S3, and S4, and then calculate the SNR, Esn, and RMSE of the four groups of signals by equations (18) and (19) and (20), respectively. Experimental indicators are shown in Figure 8.

It can be seen from Figure 8(a) that the signal-to-noise ratio of the four groups of signals after noise reduction reaches 13.73dB, and the SNR of the signal S4 after noise reduction is also 8.51dB. It can be seen from Figure 8(b) that the maximum value of the signal after the noise suppression is 92.03%, and the minimum value is 87.56%, which is close to the original signal energy. It can be seen from Figure 8(c) that the RMSE of the four sets of signals does not exceed 0.07. In order to further illustrate the noise suppression effect, we randomly selected 30 microseismic data from June to September of this coal mine for the above analysis. The SNR and Esn distribution of the microseismic signal after noise suppression are shown in Figure 9.

Figure 9 shows that after 30 microseismic signals are denoised, the SNR is between 11dB and 20dB. The 10th group signal has a maximum SNR of 19.87dB, and the

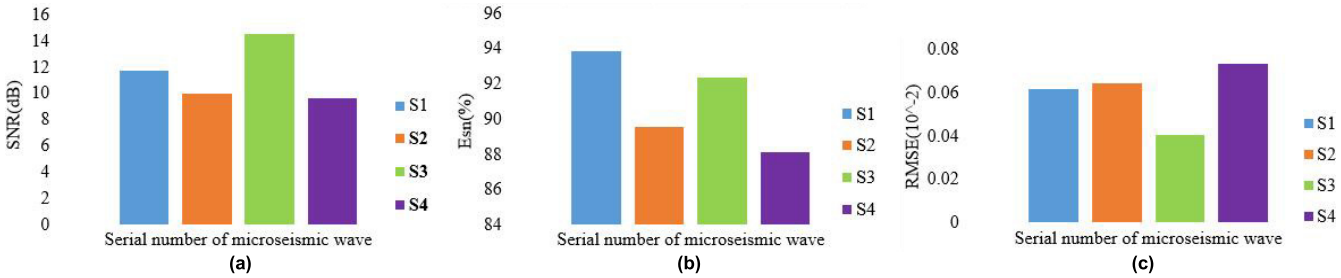

FIGURE 8. Noise suppression results of microseismic signals. (a) SNR of four microseismic signals; (b) E_{sn} of four microseismic signals; (c) RMSE of four microseismic signals.

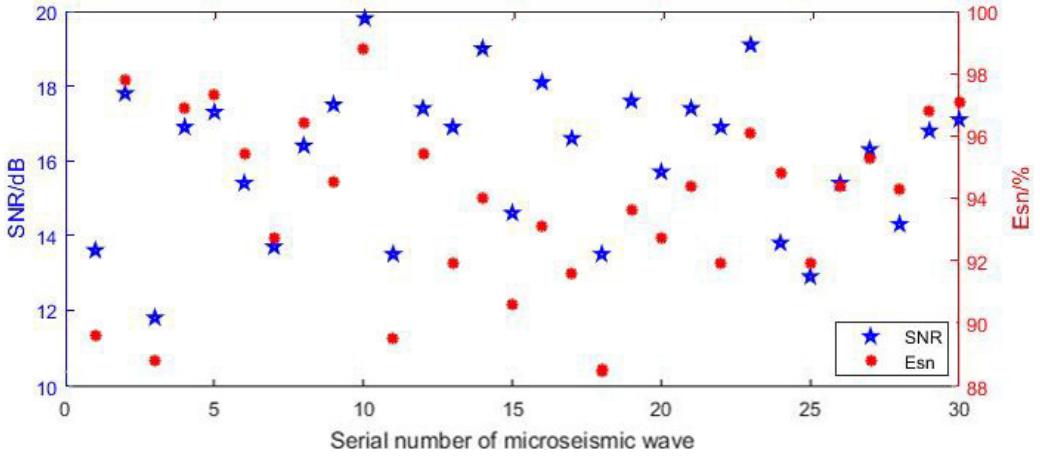

FIGURE 9. The results of noise suppression of 30 microseismic signals selected randomly by the proposed method.

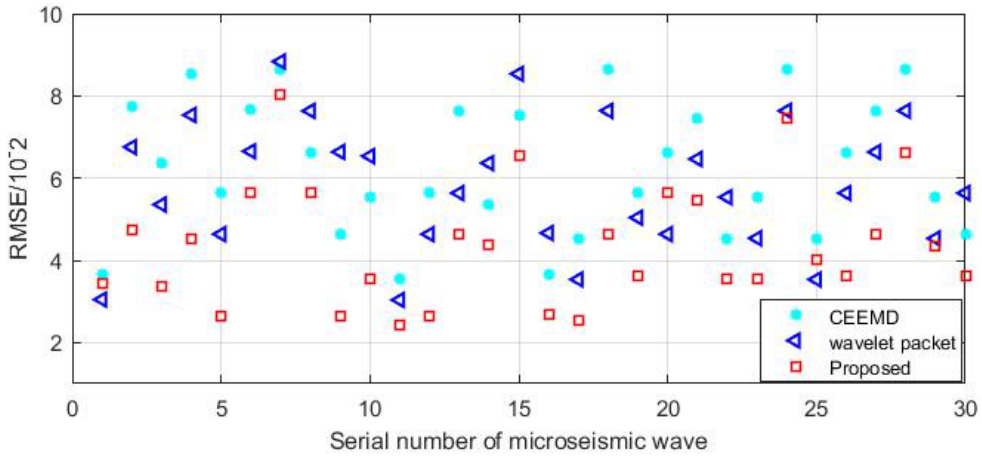

FIGURE 10. RMSE of 30 microseismic signals selected randomly after noise suppression by three different methods.

2th group signals has a minimum SNR of 11.15dB; Esn is between 89% and 99%, with the 10th group having the highest Esn of 98.82% and the 18th group having the lowest Esn of 88.35%. In order to verify the stability of the proposed method, we also calculated the distribution of the RMSE of the 30 sets of signals after noise suppression. From Figure 10, we can clearly see the overall distribution of the RMSE of the proposed method is lower than CEEMD or wavelet packet transform method. In summary, the noise suppression method based on CEEMD and wavelet packet threshold combined in this paper has a high SNR and Esn, and the validity and practicality of the noise reduction method are proved quantitatively. The method proposed by us can provide a real and effective signal source for the follow-up work of the first phase of the earthquake, the location of the source, and the interpretation of the focal mechanism.

V. CONCLUSION

Aiming at the shortcomings of the separate CEEMD decomposition method and wavelet packet threshold method, a micro-seismic signal noise suppression method based on CEEMD wavelet packet threshold is proposed. At the same time, the self-correlation function and the improved wavelet packet threshold function are introduced. After the micro seismic signal is decomposed by CEEMD, the self-correlation function is used to more accurately determine the noise of each signal by the self-correlation coefficient between the microseismic signal and the IMF obtained by the decomposition. For the larger self-correlation coefficient, wavelet is adopted. The packet threshold noise is suppressed, and finally the wavelet packet threshold noise suppressed signal and the no de-noising IMF component are reconstructed, and then a useful coal rock microseismic signal is obtained. Through experimental analysis and engineering application, it can be found that the noise suppression effect of this method is better than the single CEEMD method and wavelet packet threshold method.

REFERENCES

[1] H. Li, R. Wang, S. Cao, Y. Chen, and W. Huang, "A method for low-frequency noise suppression based on mathematical morphology in micro-seismic monitoring," *Geophysics*, vol. 81, no. 3, pp. V159–V167, 2016.

[2] Y. Chen, S. Jiao, J. Ma, H. Chen, Y. Zhou, and S. Gan, "Ground-roll noise attenuation using a simple and effective approach based on local band-limited orthogonalization," *IEEE Geosci. Remote Sens. Lett.*, vol. 12, no. 11, pp. 2316–2320, Nov. 2015.

[3] S. C. Maxwell and T. I. Urbancic, "The role of passive microseismic monitoring in the instrumented oil field," *Lead. Edge.*, vol. 20, no. 6, pp. 636–639, 2001.

[4] W. Huang, R. Wang, Y. Chen, H. Li, and S. Gan, "Damped multichannel singular spectrum analysis for 3D random noise attenuation," *Geophysics*, vol. 81, no. 4, pp. 261–270, 2016.

[5] S. Gan, S. Wang, Y. Chen, and X. Chen, "Simultaneous-source separation using iterative seislet-frame thresholding," *IEEE Geosci. Remote Sens. Lett.*, vol. 13, no. 2, pp. 197–201, Feb. 2016.

[6] Y. Chen and J. Ma, "Random noise attenuation by f-x empirical-mode decomposition predictive filtering," *Geophysics*, vol. 79, no. 3, pp. V81–V91, 2014.

[7] M. Shirzaei, W. L. Ellsworth, K. F. Tiampo, P. J. González, and M. Manga, "Surface uplift and time-dependent seismic hazard due to fluid injection in eastern Texas," *Science*, vol. 353, no. 6306, pp. 1416–1419, Sep. 2016.

[8] J. Akram and D. W. Eaton, "A review and appraisal of arrival-time picking methods for downhole microseismic data," *Geophysics*, vol. 81, no. 2, pp. KS71–KS91, Mar. 2016.

[9] S. M. Mousavi, C. A. Langston, and S. P. Horton, "Automatic microseismic denoising and onset detection using the synchrosqueezed continuous wavelet transform," *Geophysics*, vol. 81, no. 4, pp. V341–V355, Jul. 2016.

[10] N. Iqbal, A. A. Al-Shuhail, S. L. I. Kaka, E. Liu, A. G. Raj, and J. H. McClellan, "Iterative interferometry-based method for picking microseismic events," *J. Appl. Geophys.*, vol. 140, pp. 52–61, May 2017.

[11] X. F. Chen and H. M. Sun, "Seismic data denoising method based on compressed sensing theory," *Prog. Geophys.*, vol. 34, no. 4, pp. 1025–1031, 2019.

[12] Y. Gong, R. S. Jia, X. M. Lu, Y. J. Peng, W. D. Zhao, and X. L. Zhang, "To suppress the random noise in microseismic signal by using empirical mode decomposition and wavelet transform," *J. China Coal Soc.*, vol. 43, no. 11, pp. V3247–V3256, 2018.

[13] R. S. Jia, T. B. Zhao, H. M. Sun, and X. H. Yan, "Micro—Seismic signal denoising method based on empirical mode decomposition and independent component analysis," *Chin. J. Geophys.*, vol. 58, no. 3, pp. 1013–1023, 2015.

[14] W. Cao, H. M. Sun, R. S. Jia, Y. J. Cui, and X. F. Chen, "Micro-seismic signal denoising method based on wavelet packet decomposition and reconstruction," *J. Electron. Meas. Instrum.*, vol. 32, no. 4, pp. 134–143, 2018.

[15] C. Capilla, "Application of the Haar wavelet transform to detect microseismic signal arrivals," *J. Appl. Geophys.*, vol. 59, no. 1, pp. 36–46, May 2006.

[16] P. L. Mao and R. K. Aggarwal, "A novel approach to the classification of the transient phenomena in power transformers using combined wavelet transform and neural network," *IEEE Trans. Power Del.*, vol. 16, no. 4, pp. 654–660, Oct. 2001.

[17] W. Chen, J. Xie, S. Zu, S. Gan, and Y. Chen, "Multiple-reflection noise attenuation using adaptive randomized-order empirical mode decomposition," *IEEE Geosci. Remote Sens. Lett.*, vol. 14, no. 1, pp. 18–22, Jan. 2017.

[18] Y. Chen, "Dip-separated structural filtering using seislet transform and adaptive empirical mode decomposition based dip filter," *Geophys. J. Int.*, vol. 206, no. 1, pp. 457–469, 2016.

[19] W.-L. Hou, R.-S. Jia, H.-M. Sun, X.-L. Zhang, M.-D. Deng, and Y. Tian, "Random noise reduction in seismic data by using bidimensional empirical mode decomposition and Shearlet transform," *IEEE Access*, vol. 7, pp. 71374–71386, 2019.

[20] R.-S. Jia, Y.-Q. Liang, Y.-C. Hua, H.-M. Sun, and F.-F. Xia, "Suppressing non-stationary random noise in microseismic data by using ensemble empirical mode decomposition and permutation entropy," *J. Appl. Geophys.*, vol. 133, pp. 132–140, Oct. 2016.

[21] H. Zhi, J. H. Gao, and N. H. Liu, "Separation of blended seismic data using the synchrosqueezed curvelet transform," *IEEE Geosci. Remote Sens. Lett.*, to be published.

[22] N. E. Huang and Z. Wu, "A review on Hilbert-Huang transform: Method and its applications to geophysical studies," *Rev. Geophys.*, vol. 46, 2008, Art. no. RG2006.

[23] B. Demir and S. Erturk, "Empirical mode decomposition of hyperspectral images for support vector machine classification," *IEEE Trans. Geosci. Remote Sens.*, vol. 48, no. 11, pp. 4071–4084, Nov. 2010.

[24] S. M. Mousavi and C. A. Langston, "Hybrid seismic denoising using higher-order statistics and improved wavelet block thresholding," *Bull. Seismol. Soc. Amer.*, vol. 106, no. 4, pp. 1380–1393, 2016.

[25] J. Wang, Z. Li, and D. Wang, "A method for wavelet threshold de-noising of seismic data based on CEEMD," *Geophys. Prospecting Petroleum*, vol. 53, no. 2, pp. 164–172, 2014.

[26] Y. Zhao, Y. S. Yue, and J. L. Huang, "CEEMD and wavelet transform jointed de-noising method," *Progr. Geophys.*, vol. 30, no. 6, pp. 2870–2877, 2015.

[27] J. C. Hu, J. J. Lian, B. Ma, and X. F. Dong, "A de-noising and modal identification combined method based on CEEMD and wavelet packet threshold for flood discharge structures," *J. Vibrat. Shock.*, vol. 36, no. 17, pp. 1–9, 2017.

[28] L. C. Dong, X. M. Guo, and Y. N. Zheng, "Wavelet packet de-noising algorithm for heart sound signals based on CEEMD," *J. Vibrat. Shock.*, vol. 38, no. 9, pp. 192–198, 2019.

[29] W. Yu and L. Zhao, "Gravity data signal-noise separation method based on CEEMD and wavelet packet transform," *Software*, vol. 36, no. 2, pp. 49–54, 2015.

[30] M. Yang, J. Wang, X. Zhou, and Q. Guo, "De-noising method based on CEEMD and wavelet packet," *J. Nanjing Univ. Posts Telecommun.*, vol. 38, no. 2, pp. 41–47, 2019.

[31] H. Zhang, Y. Fu, L. B. Feng, Y. Zhang, and R. Hua, "Implementation of hybrid alignment algorithm for protein database search on the SW26010 many-core processor," *IEEE Access*, vol. 7, pp. 128054–128063, 2019.

[32] S. G. Chang, B. Yu, and M. Vetterli, "Adaptive wavelet thresholding for image denoising and compression," *IEEE Trans. Image Process.*, vol. 9, no. 9, pp. 1532–1546, Sep. 2000.

[33] P. Gerstoft, K. G. Sabra, P. Roux, W. A. Kuperman, and M. C. Fehler, "Green's functions extraction and surface-wave tomography from microseisms in southern California," *Geophysics*, vol. 71, no. 4, pp. SI23–SI31, 2006.

[34] H. X. Shao and H. F. Gao, "Improved wavelet threshold denoising method for processing FBG sensing signals," *Laser Infrared*, vol. 44, no. 1, pp. 73–76, 2014.

[35] D. Bykhovsky, "Simple generation of gamma gamma-gamma and K distributions with exponential self-correlation function," *J. Lightw. Technol.*, vol. 34, pp. 2106–2110, May 2016.